Defects and Domain Boundaries in Self-Assembled Terephthalic Acid (TPA) Mono layers on CVD-Grown Graphene on Pt(111)

ARTICLE *in* LANGMUIR · APRIL 2013

Impact Factor: 4.46 · DOI: 10.1021/la400972k · Source: PubMed

2 AUTHORS:

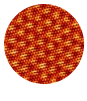

Rafik Addou
University of Texas at Dallas
39 PUBLICATIONS **436** CITATIONS
SEE PROFILE

Matthias Batzill
University of South Florida
116 PUBLICATIONS **4,369** CITATIONS
SEE PROFILE

Langmuir

Article

pubs.acs.org/Langmuir

Defects and Domain Boundaries in Self-Assembled Terephthalic Acid (TPA) Monolayers on CVD-Grown Graphene on Pt(111)

Rafik Addou and Matthias Batzill*

Department of Physics, University of South Florida, Tampa, Florida 33620, United States

ABSTRACT: Self-assembly of terephthalic acid (TPA), vacuum deposited on Pt(111) supported graphene, has been investigated by scanning tunneling microscopy (STM). TPA organizes in an ordered 3 × 4 superstructure with respect to the graphene lattice. This structure is a consequence of hydrogen-bonded TPA chains that arrange in a commensurate overlayer on graphene. Due to the polycrystalline nature of graphene on Pt(111), the TPA layer exhibits various grain boundaries and dislocations. Molecular resolved STM imaging has been used to characterize these defect structures in the TPA monolayer.

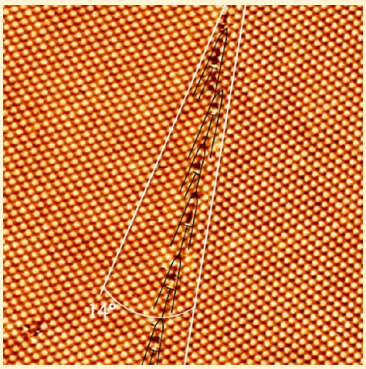

1. INTRODUCTION

Organic monolayers are of increasing interest for functionalizing graphene for chemical recognition, organic−inorganic hybrid materials, and electronic devices.[1−8] One important category of self-ordered organic monolayers is that where strong intermolecular interactions, such as hydrogen bonding, cause self-organization of molecules in a precise pattern. Interactions to the substrate (here graphene) are typically weak van der Waals interactions. However, the substrate−molecule interaction can be strong enough to force the molecular adlayer to adsorb at specific substrate adsorption sites and form a commensurate overlayer with respect to graphene.

One molecule that has been demonstrated to self-organize on inert surfaces such as Au(111),[9] Ag(111),[10] Cu(100),[11,12] or graphite HOPG(0001)[13,14] is terephthalic acid (TPA). The two carboxylic acid groups of TPA can interact with neighboring TPA molecules via hydrogen bonding forming linear chains. Furthermore, interactions between molecules in adjacent TPA chains result in a two dimensionally ordered overlayer structure. While on strongly interacting substrates dehydrogenation of the carboxylic acid can cause covalent bonding between TPA and the substrate, the interaction between TPA and graphene is expected to be only due to van der Waals forces due to the inert nature of graphene. Therefore on graphene no dehydrogenation of TPA is expected, and indeed recent near edge X-ray absorption fine structure (NEXAFS) and X-ray photoemission spectroscopy (XPS) studies of TPA adsorption on graphene/Ni(111) surfaces confirmed that TPA stays intact and adopts a flat lying configuration, i.e. the phenyl ring is almost parallel to the graphene surface.[15] Furthermore, studies of TPA adsorption of HOPG(0001) in solution[13] indicated the formation of a commensurate ordered overalyer of flat TPA molecules.

Although graphene only interacts weakly with Pt(111) and therefore maintains many of its characteristic physical properties, i.e. electronic[16] and phonon[17] structure, of freestanding graphene, there also exist differences between Pt-supported graphene and HOPG. For instance, the lattice mismatch between graphene and Pt(111) induces the formation of many different rotational domains with each of them forming specific moiré superstructures.[18] Influence of moiré structures in metal supported graphene on molecular adsorption has been previously reported.[19] One question to answer in this study is, therefore, if the moiré structure modifies the adsorption site of TPA, i.e. do different domains exhibit different TPA structures, or are the TPA adsorption sites controlled by the graphene atomic lattice only. Furthermore, the multiple rotational domains of graphene imply that commensurate TPA adlayers will also form domain boundaries or otherwise would become incommensurate as the growth front crosses substrate domain boundaries. This raises the fundamental question of how substrate domain boundaries affect the organic monolayer morphology. In particular, what kind of substrate-induced domain boundaries are observed in a TPA monolayer?

Here we use room-temperature scanning tunneling microscopy (STM) to investigate the morphology and defects in monolayer TPA with molecular resolution. This enables us to show that the graphene−TPA interaction is strong enough to force the TPA layer in registry with individual graphene domains with no influence from the moiré structure in the graphene. The rotationally misaligned grains in the polycrystalline graphene induces one-dimensional small- and large-angle

Received: March 14, 2013
Revised: April 25, 2013
Published: April 29, 2013

dx.doi.org/10.1021/la400972k | *Langmuir* 2013, 29, 6354−6360

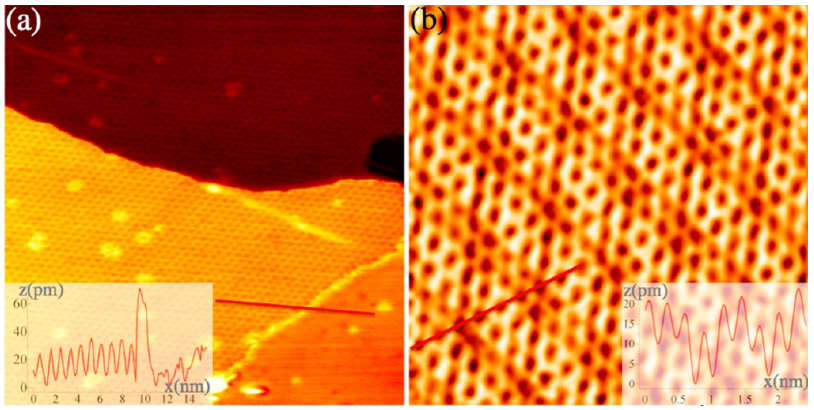

Figure 1. STM image of graphene monolayer on Pt(111). In (a) a 40 × 40 nm^2 area is imaged (V_{bias} = 150 mV, I_t = 1.8 nA), showing an atomic step in the Pt substrate and a graphene domain boundary in the lower right corner. The periodic pattern in the upper left domain is a moiré pattern of the rotated graphene sheet on Pt(111). The moiré structure of the domain in the lower right corner is less pronounced, due to a different rotation angle. Note the bright contrast at the domain boundary. A high-resolution STM image (V_{bias} = 7 mV, I_t = 2 nA) is shown in (b). Both the hexagonal carbon lattice and a long-range periodic modulation due to the underlying Pt(111) substrate can be discerned. Line-profiles along the indicated lines show the corrugation of the moiré structure in (a) and the atomic lattice in (b).

grain boundaries in the TPA overlayer, which we characterize by STM.

2. EXPERIMENTAL METHODS

All the experiments were conducted in a single UHV chamber equipped with a scanning tunneling microscope (STM) and low-energy electron diffraction optics (LEED). The Pt(111) single crystal sample was cleaned by Ar-ion sputtering and annealing cycles, followed by annealing in 10^{-6} Torr oxygen and final flashing in vacuum. Graphene was grown on the Pt(111) crystal by exposure to 5 × 10^{-7} Torr ethylene for 5 min with the sample held at a temperature of 750 °C. The graphene layer was characterized by LEED and STM, both indicating the formation of multiple rotational domains of graphene. The graphene-covered surface is extremely unreactive and samples can even be transported through air without any indication of surface contamination after a brief annealing to 500 °C. TPA was deposited on the graphene/Pt(111) sample by thermal evaporation. The TPA evaporator consisted of a Ta-boat with a pinhole to release the TPA vapor. The Ta-boat was heated by direct current heated Ta-wires. For evaporation of TPA, a temperature of the Ta-boat of ∼137 °C was used, measured by a thermocouple spot-welded to the boat. To minimize contamination of the main analysis chamber the TPA deposition was conducted in the modified load-lock of the UHV system. The load lock was pumped with a turbo pump and had a base pressure of better than 10^{-8} Torr. TPA deposition was carried out with the sample at room temperature.

LEED characterization of the TPA overlayer was not possible because of a rapid electron-beam induced desorption of TPA. Thus, only STM has been used to characterize the structure of adsorbed TPA on the molecular level.

3. RESULTS AND DISCUSSION

Graphene on Pt(111) forms many different rotational domains and this has been thoroughly characterized before.[8,16,18] Figure 1 shows STM images of such a graphene overlayer on Pt(111) with two rotationally misaligned grains visible in (a) and a high-resolution image of a single grain in (b). Because of the lattice mismatch between graphene and Pt(111) and because of the different rotational alignments between the graphene and platinum lattices moiré superstructures are formed. Depending on the graphene preparation, atomic-scale defects in the graphene layer and at the domain boundaries are present that appear as bright protrusions in STM images. The defects at the grain boundary can be used as markers to identify locations of graphene boundaries, which can be used to find grain boundaries in the graphene even when it is covered by TPA as we show below. The unit-cell of the graphene moiré superstructure corresponds to carbon atoms in the graphene occupying different lattice sites on the Pt(111) surface. Thus the moiré structure is a superimposed periodicity in the graphene induced by the lattice mismatch with the Pt substrate. If this additional moiré superstructure was playing an important role in the ordering of a self-assembled TPA monolayer on Pt/graphene, then different TPA unit cells for different graphene/Pt(111) grains would be expected. This is, however, not the case and only a single TPA unit cell has been observed. Furthermore, the unit cell we derive from our STM measurements (see below) is identical to the unit cell that has been reported for TPA on HOPG in solution.[13] Therefore, we conclude that the adsorption sites of TPA on graphene supported on Pt(111) are not altered by the platinum substrate. It is also worth pointing out that the moiré structure of the graphene substrate cannot be resolved in STM when TPA covers the surface. This is similar to the case where the surface has been covered by an inorganic monolayer.[20]

Figure 2 shows a high-resolution image of TPA on graphene/Pt(111). Depending on the imaging conditions of the tip and/or tunneling parameters, TPA is imaged in an elongated shape or almost round. For the elongated shape, the long axis in the STM image corresponds to the long axis of the molecule. From the STM image we can measure the unit cell as 9.8 ± 0.6 Å along the TPA long axis and 7.4 ± 0.3 Å for the unit cell vector connecting neighboring TPA chains. The angle between these two unit cell vectors is measured to 60°.

For a TPA layer that is commensurate with the graphene substrate, i.e. every TPA molecule has the same adsorption site on graphene, the unit cell can be refined by using the graphene lattice to define discrete unit-cell vectors that can be matched with the measured unit cells. The lattice vectors with the best match to the measurements are shown in Figure 2b. This unit cell may be expressed as a 3 × 4 unit cell with respect to the graphene lattice, i.e. 7.38 Å × 9.84 Å. This unit cell is equivalent to the unit cell reported for solution-deposited TPA on HOPG.[13] The dimensions of the TPA unit cell on graphene can be compared to values derived for TPA monolayers on other "inert" substrates. The TPA−TPA chain distance was

dx.doi.org/10.1021/la400972k | Langmuir 2013, 29, 6354−6360

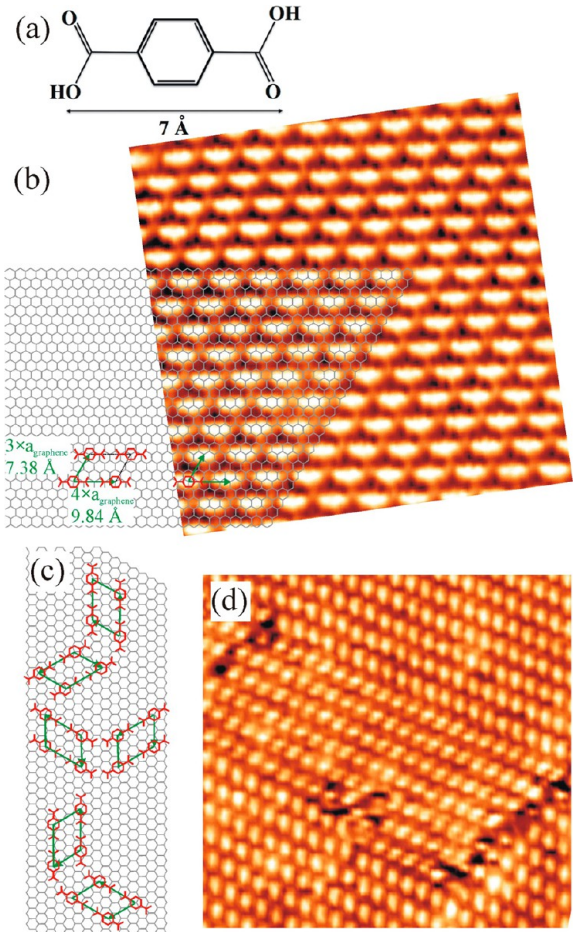

Figure 2. Molecular structure of TPA on graphene. (a) Model of TPA molecule. (b) STM image (V_{bias} = 1.5 V, I_t = 1 nA) of TPA monolayer with graphene lattice superimposed. The 3 × 4 unit cell of TPA is indicated (note: the adsorption site of TPA relative to the graphene lattice is unknown). All six equivalent unit-cell structures that are expected to exist on single crystal graphene substrate are indicated in (c). Two mirrored unit cells may form twin boundaries as shown in the STM image (V_{bias} = 1.5 V, I_t = 1 nA) in (d).

reported to 10 ± 0.5 Å for Ag(111)[10] and 10.1 ± 0.3 Å for Au(111).[9] Individual hydrogen-bonded TPA chains were also observed on Pd(111) with a separation of 9.5 Å.[21] These distances are close to the TPA unit cell vector on graphene of 9.84 Å. With a molecule length of 7 Å the unit cell vector along the TPA chain then suggests a H-bonding distance (oxygen-to-oxygen) of ∼2.8 Å. This H-bond length is just a little longer than the distance reported for bulk TPA crystals of 2.7 Å.[22] For the separation between TPA chains we obtain 7.38 Å × sin 60° = 6.39 Å which can be compared to reported values of 6.1 ± 0.5 Å and 6.1 ± 0.3 Å for TPA on Ag(111) and Au(111), respectively.

The symmetry of the unit cell suggests the existence of multiple rotational graphene domains even on single crystalline graphene and the formation of twin domains as indicated in Figure 2c. However, twins are rarely observed in STM, most likely because of the energy cost associated with the broken hydrogen bonds at the twin-domain boundary. Nevertheless, in Figure 2d we have observed a small twin domain embedded in a single TPA domain. This observation gives additional validity to the structural model.

To form a commensurate overlayer, a significant interaction between graphene and TPA must exist that "pins" TPA to a preferred adsorption site on graphene. The interplay between substrate interactions, intermolecular in-chain hydrogen bonding, and intermolecular across-chain electrostatic interaction determines the ordering of the TPA film. It is, however, not possible to determine the adsorption sites of the TPA molecules on graphene from the STM images. In the following we discuss defects in the TPA layer, in particular defects induced by substrate defects, such as tilt domains in the graphene layer.

3.1. Incomplete Monolayers. For submonolayer coverage, two regions can be differentiated. One surface region cannot be resolved by STM at room temperature. This region presumably consists of fast diffusing TPA in a lattice gas and/or consists of TPA molecules that can be easily moved by the STM tip. The other regions are crystalline TPA islands with the structure described above for monolayer coverage. Thus these TPA islands are ordered TPA domains that are in equilibrium with a disordered TPA lattice-gas that surrounds them. Interestingly, the TPA domains seem to be undisturbed by any step-edges present at the surface, as is evident from the STM image shown in Figure 3a. These step edges are steps on the Pt(111) surface. However, since graphene grows over step edges on Pt and other transition metal substrates in a "carpet" growth mode,[8,16,23] there are actually no sharp step edges present in the graphene overlayer. Consequently the TPA molecules "see" a smooth graphene surface without steps. This explains why the Pt substrate step edges do not influence the TPA grain structure. The growth of other organic molecules over substrate step edges on graphene supported on SiC has been previously reported[24] and thus the observation of the formation of grain structures that seamlessly bridge substrate step edges is a convenient way to demonstrate that graphene covers the substrate uniformly.

For the individual TPA islands it is also apparent that different possible island edge orientations are not equally frequent. Island edges that correspond to the direction of hydrogen-bonded TPA chains are the most frequent orientation as shown in Figure 3b. The lower edge energy for hydrogen-bonded TPA chains compared to the "unsaturated" carboxylic acid termination is in agreement with the notion of lowering of the energy due to hydrogen bond formation along the chains and is in agreement with those computed for two-dimensional TPA islands that found a binding energy difference of 0.22 eV between a carboxylic terminated edge versus one that is hydrogen bonded.[14] Because graphene forms a polycrystalline layer on Pt(111) with individual grains ranging from tens to hundreds of nanometers we can also observe a variety of TPA domain orientations. For incomplete monolayer this causes domain boundaries that are fairly open in structure, presumably to minimize the number of non-hydrogen bond terminated carboxylic acid groups. Also, in Figure 3b it is apparent that the TPA layer does not necessarily switch abruptly from one orientation to the other. Instead the TPA may form intermediate orientations. This intermediate orientation can be understood by (partially) maintaining hydrogen bonding between molecules and such presents a mechanism to reduce the grain boundary energy. This gradual reorientation of the molecules is possible because of weak interactions between TPA and graphene. In the structure shown in Figure 3b the TPA chains in the grain boundary can be fitted onto segments of a circle with a radius of

dx.doi.org/10.1021/la400972k | Langmuir 2013, 29, 6354−6360

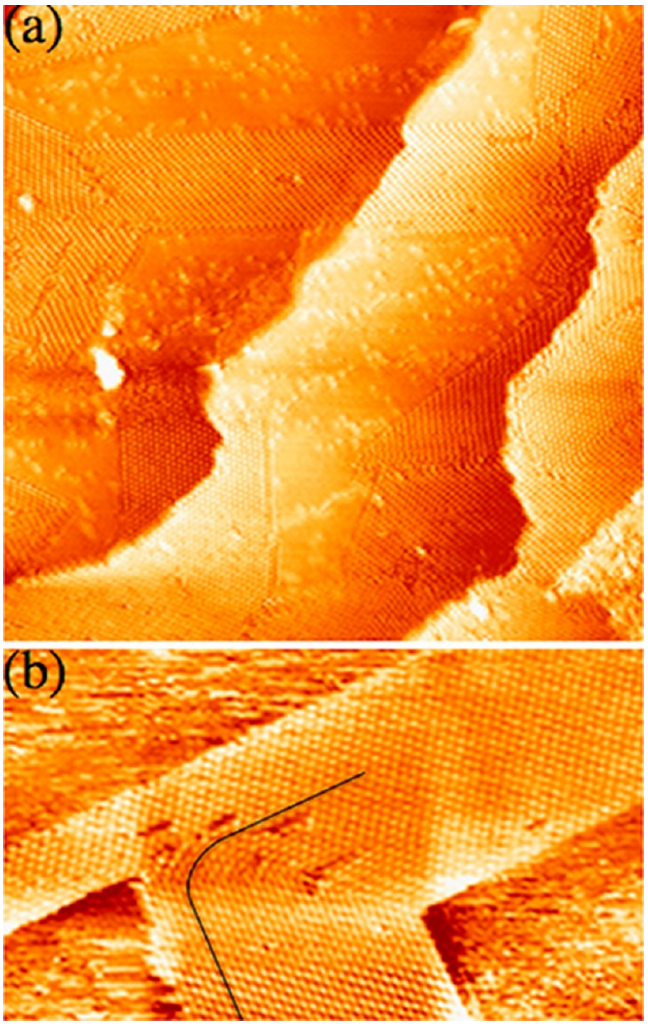

Figure 3. Partial monolayer of TPA on graphene/Pt(111). In (a) an 75 × 75 nm^2 area is shown (V_{bias} = 1.2 V, I_t = 2 nA). Ordered TPA islands easily grow across substrate step edges indicating that the graphene, like a carpet, lies across the Pt-step edges forming a uniform substrate for the TPA to grow on. In (b) a domain boundary between two tilted TPA islands is shown. For the lower coverage the TPA molecules in the domain boundary are less densely packed and a gradual reorientation of the TPA-molecule chain that connects the two TPA islands can be observed in the grain boundary. A single TPA chain is highlighted by the solid line.

approximately 5 nm. Placing TPA molecules on a circle rather than a straight line necessarily compresses one hydrogen bond and extends the other. For a 5-nm radius this variation is ±0.1 Å, i.e. instead of a hydrogen bond length of 2.8 Å one will be 2.7 Å and the other one will be 2.9 Å. This falls within the above-discussed range of previously observed hydrogen bond lengths of TPA on various substrates and this suggests that such a bending radius of the TPA chains is energetically reasonable. We point out that this more open grain boundary structure is only observed for low TPA coverage, i.e. incomplete monolayers. Even for incomplete layers this structure is observed in less than 10% of the domain boundaries. It is uncertain, however, if the rarity of these boundaries is related to the energy cost or growth kinetics.

In the following we describe defects in the TPA film that are mainly a consequence of the polycrystalline graphene substrate which causes rotated TPA layers to form. These defects can be categorized as (i) individual point defects due to insertion of "half-chains" of TPA (this is equivalent to edge-dislocations in 3D materials) and (ii) tilt grain boundaries between TPA grains with different rotation.

3.2. Dislocations in TPA Monolayer. It may be worth pointing out that there exist very basic differences for dislocations in a bulk material compared to a two-dimensional atomic or molecular layer. In a bulk material the dislocation line and the Burgers vector define a dislocation, and their relative orientation to each other gives rise to different kinds of dislocations (e.g., screw or edge dislocation). For a 2D material the Burgers vector has to lie within the surface plane and the dislocation line may be viewed as a surface normal vector, i.e. in terms of bulk materials only edge dislocations can be observed in 2D materials. Figure 4 shows two kinds of dislocation cores

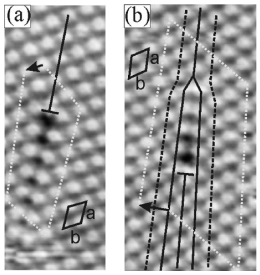

Figure 4. Dislocation cores in TPA monolayer on graphene. (a) Single edge dislocation with Brugers circuit (white dashed line) indicating a Burgers vector **b** (see indicated unit cell). (b) Dislocation complex with a Burgers vector of **a** + 2**b**, as indicated by the Burgers circuit.

that have been observed in a TPA monolayer on graphene. The dislocation in Figure 4a may be described by the insertion of a TPA half-chain (equivalent to a crystal half-plane in bulk materials) in the TPA lattice. The Burgers vector can be determined with the so-called Burgers circuit. This analysis yields a Burgers vector with length and direction of the TPA unit cell vector **b** = 3 × $a_{graphene}$. The dislocation shown in Figure 4b is more complex and may be described as a combination of two dislocations. One is again due to the insertion of a TPA half-chain. The second dislocation exists in the more open packed region of the first dislocation core. The open packing enables the splitting of a single TPA chain into two chains. A Burgers circuit surrounding this dislocation complex reveals that this dislocation complex exhibits a Burgers vector of **a** + 2**b** (in terms of TPA unit cell vectors **a** and **b**). Formation of a longer Burgers vector generally costs energy, since the strain energy in the dislocation increases with the square of the length of the Burgers vector.[25] Thus dislocations with Burgers vectors longer than a unit cell vector are not commonly observed in most materials. The fact that we observe dislocations with longer Burgers vector may be a consequence of (i) the lower strain energies due to the distortion of the lattice in the molecular crystal compared to atomic crystals and (ii) intermolecular interactions in the dislocation core that can energetically compensate for the increased strain energy.

3.3. Grain Boundaries. TPA forms a commensurate overlayer with graphene. Thus on a single-crystalline graphene only 3 rotational TPA variants with the TPA chains rotated 0, 60, and 120 degrees should exist. In addition, each of these rotational variants may be mirrored, so that a total of 6 symmetry domains exist on a single graphene grain. These variants are indicated in Figure 2c. Thus on a single crystal

dx.doi.org/10.1021/la400972k | *Langmuir* 2013, 29, 6354−6360

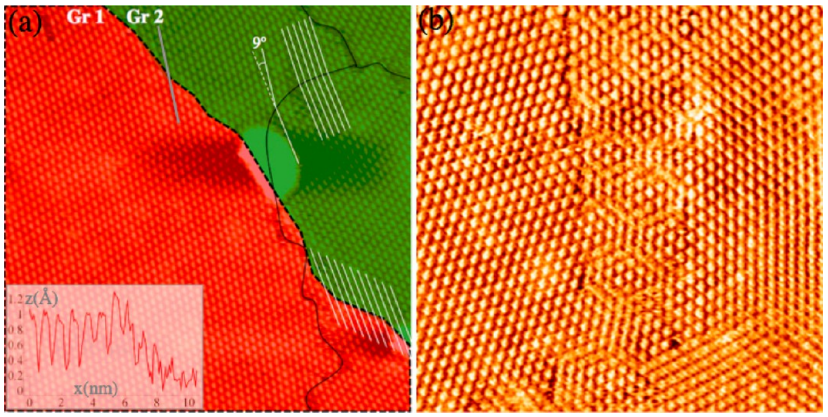

Figure 5. STM images of TPA grain boundaries. The STM image (V_{bias} = 1.5 V, I_t = 1 nA) in (a) demonstrates that TPA domains can cross graphene grain boundaries. The red and green areas represent two graphene grains separated at the dashed line. A line profile across this grain boundary is shown indicating the corrugation of the TPA molecules. The graphene grain boundary was identified by the increased height in STM images at graphene grain boundaries (see also Figure 1a). There are three TPA domains with their boundaries indicated by the solid line in this image, with two rotated by 9° relative to each other. It is apparent that both of these TPA domains are crossing the underlying graphene grain boundary, thus indicating that the interaction between the graphene and TPA is small enough to allow growth of TPA on graphene with an arbitrary orientation to some extent. The STM image in (b) shows an unusual domain boundary that has only been observed once. Rather than exhibiting a line defect at the grain boundary the grain boundary extends over tens of nanometers laterally. Within the grain boundary the TPA molecules arrange not just in linear TPA chains but form a more complex structure. Apparently such a "dissociated" domain boundary can minimize the grain boundary energy for certain tilt angles between TPA domains.

graphene there would only exist a limited number of well-defined TPA-domain boundaries, as for example shown in Figure 2d. In addition, however, our graphene sample is polycrystalline, which gives rise to almost arbitrary rotations of TPA domains and thus arbitrary tilt-domain boundaries.

TPA overlayers nucleated in one graphene grain will eventually grow across graphene grain boundary and thus loosen its registry with the graphene substrate. The extent to which it keeps growing with the same orientation will depend on the energy cost of not being in its favorable orientation with respect to the graphene substrate. Either the growing TPA island will rotate to regain the proper alignment with the substrate or the island ceases to grow because of the additional energy cost for growing out of registry with the graphene substrate. In the latter case the island boundary will eventually collide with another TPA island and grain boundaries of rotationally misaligned TPA islands will form. Grain boundaries in graphene sometimes exhibit elevated contrast, or "clusters" of elevated contrast along the boundary (see Figure 1a). These clusters of elevated contrast can be used as markers to identify the location of the graphene grain boundaries even after it has been covered with TPA. In Figure 5a we clearly can identify a grain boundary of the underlying graphene and the domain boundaries in the TPA film. It is apparent that the domain boundaries of substrate and overlayer follow each other closely but do not exactly overlap. This is an indication of the fairly weak TPA/graphene interaction that allows growing TPA islands to maintain their orientation even as the underlying graphene changed its orientation and thus is out of registry with the TPA layer.

In the following we characterize TPA domain boundaries in analogy to bulk materials as small and large angle grain boundaries.

3.3.1. Small Angle Domain Boundaries. In bulk materials, small angle grain boundaries can be represented as a series of dislocation lines. For a 2D material with different rotational misalignments between individual grains the boundaries are best described as tilt domain boundaries (rather than twist boundaries which necessitate layers on top of each other). Small angle tilt boundaries are described by a periodic arrangement of inserted crystal half-planes that terminate at edge dislocations. In a 2D material the equivalent is the insertion of an extra TPA half-chain. In Figure 6a we

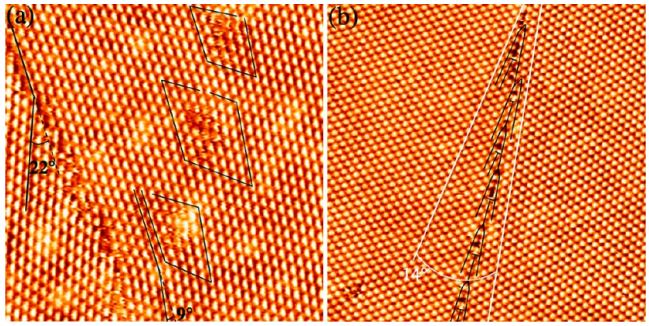

Figure 6. STM images (V_{bias} = 1.5 V, I_t = 1 nA) of regular domain boundaries in TPA monolayers. In (a) two domain boundaries are present: (i) a small angle domain boundary, with a tilt angle between domains of ~9°. It consists of individual edge dislocations as indicated by the Burgers circuits around the dislocation cores; and (ii) a large angle domain boundary with a tilt angle of 22° between domains. In (b) a single domain boundary is imaged with 14° tilt angle between domains. This domain boundary may still be categorized as a small angle grain boundary as it is constructed by a line of dislocation cores of the kind shown in Figure 4b.

demonstrate the existence of such small angle domain boundaries in TPA monolayers. The two domains are rotated by ~9° relative to each other. We perform a Burgers circuit around dislocation cores to determine the Burgers vector as **b**, similar to the case of the individual dislocation shown in Figure 4a, although the dislocation core could not be resolved in Figure 6a.

In Figure 6b a small angle grain boundary with tilt angle of 14° is observed. For a 14° angle a high density of dislocation

dx.doi.org/10.1021/la400972k | *Langmuir* 2013, 29, 6354−6360

cores is required. Also in this case the dislocations are of the kind shown in Figure 4b and thus have a larger Burgers vector.

3.3.2. Large Angle Domain Boundaries. If the tilt angle between individual grains is too large to induce the rotation by a series of edge dislocations, large angle grain boundaries are observed. Figure 6a shows a typical representation of a large angle domain boundary (in addition to the small angle boundary that is discussed above) with the two grains rotated by ∼22°. The boundary consists largely of the molecules occupying the respective lattice points of their grains and only rarely molecules appear to occupy positions that are not part of any of the two lattices. It is also obvious that grain boundaries are arranged such that most of the molecules in the grain boundary are part of hydrogen-bonded TPA chains rather than unsaturated edges. In the large angle domain boundary shown in Figure 6a we can also identify individual TPA molecules that belong to both domains and appear to be completely hydrogen bonded to one domain on one side and the other domain on the other side.

An interesting observation of a special grain boundary is shown in Figure 5b. It appears that for certain grain orientations the system may find another way to reduce grain boundary energy. In this case, instead of forming a grain boundary along a line in the crystal, a complex interface structure between two grains is formed that extends over several nanometers. Thus such a grain boundary may be described as an extended two-dimensional defect. Effects of dissociation of grain boundaries to lower the grain boundary energy are also known for certain bulk materials.[26] However, for the case of the TPA layer the exact structure of the interface is yet to be determined.

4. SUMMARY

TPA on graphene adsorbs in a commensurate overlayer with a 3×4 unit cell relative to graphene. TPA stays intact and forms hydrogen-bonded chains with a TPA−TPA distance of 9.84 Å. Neighboring TPA chains are separated by 6.39 Å. Pt substrate-induced moiré structure in graphene does not modify the adsorption of TPA. The adsorption structure of TPA on graphene is similar to that on Ag(111) or Au(111) surfaces.

The multiple rotational domains of graphene on Pt(111) enable a study of grain boundary formation in 2D TPA layers. Formation of both small angle grain boundaries, consisting of a series of edge dislocations, and large angle grain boundaries has been observed. In the large angle grain boundaries hydrogen-bonded TPA chains are preferred over "unsaturated" carboxylic-acid groups, in agreement with the notion that hydrogen bonding reduces edge energies of graphene islands. In rare occasions, a special grain boundary configuration is observed. These grain boundaries are extended to a width of several tens of nanometers that enables a gradual rotation of the TPA chains from one grain to the other without the formation of abrupt edges. In conclusion the study presented here demonstrates that STM imaging of a two-dimensional molecular adlayer on polycrystalline graphene is a powerful tool to visualize grain boundary formation and structure of 2D self-assembled molecular films.

AUTHOR INFORMATION

Notes

The authors declare no competing financial interest.

ACKNOWLEDGMENTS

Financial support from the National Science Foundation under award NSF-DMR 1204924 is acknowledged.

REFERENCES

(1) Wang, Q. H.; Hersam, M. C. Room-temperature molecular-resolution characterization of self-assembled organic monolayers on epitaxial graphene. *Nat. Chem.* **2009**, *1*, 206.
(2) Colson, J. W.; Woll, A. R.; Mukherjee, A.; Levendorf, M. P.; Spitler, E. L.; Shields, V. B.; Spencer, M. G.; Park, J.; Dichtel, W. R. Oriented 2D covalent organic framework thin films on single-layer graphene. *Science* **2011**, *332*, 228.
(3) Zhang, H. G.; Sun, J. T.; Low, T.; Zhang, L. Z.; Pan, Y.; Liu, Q.; Mao, J. H.; Zhou, H. T.; Guo, H. M.; Du, S. X.; Guinea, F.; Gao, H.-J. Assembly of iron phthalocyanine and pentacene molecules on graphene monolayer grown on Ru(0001). *Phys. Rev. B* **2011**, *84*, 245436.
(4) Martínez-Galera, A. J.; Gómez-Rodríguez, J. M. Surface diffusion of simple organic molecules on graphene on Pt(111). *J. Phys. Chem. C* **2011**, *115*, 23036.
(5) Hlawacek, G.; Khokhar, F. S.; van Gastel, R.; Poelsema, B.; Teichert, Ch. Smooth growth of organic semiconductor films on graphene for high-efficiency electronics. *Nano Lett.* **2011**, *11*, 333.
(6) Alaboson, J. M. P.; Wang, Q. H.; Emery, J. D.; Lipson, A. L.; Bedzyk, M. J.; Elam, J. W.; Pellin, M. J.; Hersam, M. C. Seeding atomic layer deposition of high-k dielectrics on epitaxial graphene with organic self-assembled monolayers. *ACS Nano* **2011**, *5*, 5223.
(7) Huang, H.; Chen, S.; Gao, X.; Chen, W.; Wee, A. T. S. Structural and electronic properties of PTCDA thin films on epitaxial graphene. *ACS Nano* **2009**, *3*, 3431.
(8) Batzill, M. The surface science of graphene: Metal interfaces, CVD synthesis, nanoribbons, chemical modifications, and defects. *Surf. Sci. Rep.* **2012**, *67*, 83.
(9) Clair, S.; Pons, S.; Seitsonen, A. P.; Brune, H.; Kern, K.; Barth, J. V. STM study of terephthalic acid self-assembly on Au(111): Hydrogen-bonded sheets on an inhomogeneous substrate. *J. Phys. Chem. B* **2004**, *108*, 14585.
(10) Suzuki, T.; Lutz, Th.; Payer, D.; Lin, N.; Tait, S. L.; Costantini, G.; Kern, K. Substrate effect on supramolecular self-assembly: From semiconductors to metals. *Phys. Chem. Chem. Phys.* **2009**, *11*, 6498.
(11) Ge, Y.; Adler, H.; Theertham, A.; Kesmodel, L. L.; Tait, S. L. Adsorption and bonding of first layer and bilayer terephthalic acid on theCu(100) surface by high-resolution electron energy loss spectroscopy. *Langmuir* **2010**, *26*, 16325−16329.
(12) Tait, S. L.; Lim, H.; Theertham, A.; Seidelz, P. First layer compression and transition to standing second layer of terephthalic acid on Cu(100). *Phys. Chem. Chem. Phys.* **2012**, *14*, 8217−8223.
(13) Lackinger, M.; Griessl, S.; Market, T.; Jamitzky, F.; Heckl, W. M. Self-assembly of benzene-dicarboxylic acid isomers at the liquid solid interface: Steric aspects of hydrogen bonding. *J. Phys. Chem. B* **2004**, *108*, 13652−13655.
(14) Lackinger, M.; Griessl, S.; Kampschulte, L.; Jamitzky, F.; Heckel, W. M. Dynamics of grain boundaries in two-dimensional hydrogen-bonded molecular networks. *Small* **2005**, *1*, 532−539.
(15) Zhang, W.; Nefedov, A.; Naboka, M.; Cao, L.; Wöll, Ch. Molecular orientation of terephthalic acid assembly on epitaxial graphene: NEXAFS and XPS study. *Phys. Chem. Chem. Phys.* **2012**, *14*, 10125−10131.
(16) Sutter, P.; Sadowski, J. T.; Sutter, E. Graphene on Pt(111): Growth and substrate interaction. *Phys. Rev. B* **2009**, *80*, 245411.
(17) Politano, A.; Marino, A. R.; Formoso, V.; Chiarello, G. Evidence of Kohn anomalies in quasi-freestanding graphene on Pt(111). *Carbon* **2011**, *50*, 734−736.
(18) Merino, P.; Švec, M.; Pinardi, A. L.; Otero, G.; Martín-Gago, J. A. Strain-driven moiré superstructures of epitaxial graphene on transition metal surfaces. *ACS Nano* **2011**, *5*, 5627.
(19) Pollard, A. J.; Perkins, E. W.; Smith, N. A.; Saywell, A.; Goretzki, G.; Phillips, A. G.; Argent, S. P.; Sachdev, H.; Müller, F.; Hüfner, S.;

Gsell, S.; Fischer, M.; Schreck, M.; Osterwalder, J.; Greber, T.; Berner, S.; Champness, N. R.; Beton, P. H. Supramolecular Assemblies Formed on an Epitaxial Graphene Superstructure. *Angew. Chem., Int. Ed.* **2010**, *49*, 1794−1799.
(20) Addou, R.; Dahal, A.; Batzill, M. Growth of a two-dimensional dielectric monolayer on quasi-freestanding graphene. *Nat. Nanotechnol.* **2013**, *8*, 41−45.
(21) Cañas-Ventura, M. E.; Klappenberger, F.; Clair, S.; Pons, S.; Kern, K.; Brune, H.; Strunskus, T.; Wöll, Ch.; Fasel, R.; Barth, J. V. Coexistence of one- and two-dimensional supramolecular assemblies of terephthalic acid on Pd(111) due to self-limiting deprotonation. *J. Chem. Phys.* **2006**, *125*, 184710.
(22) Śledź, M.; Janczakm, J.; Kubiak, R. New crystalline modification of terephthalic acid. *J. Mol. Struct.* **2001**, *595*, 77.
(23) Addou, R.; Dahal, A.; Sutter, P.; Batzill, M. Monolayer graphene growth on Ni(111) by low temperature chemical vapor deposition. *Appl. Phys. Lett.* **2012**, *100*, 021601.
(24) Huang, H.; Chen, S.; Gao, X.; Chen, W.; Wee, A. T. S. Structural and electronic properties of PTCDA thin films on epitaxial graphene. *ACS Nano* **2009**, *3*, 3431−3436.
(25) See for example Kittel, C. *Introduction to Solid State Physics*, 8th ed.; John Wiley & Sons, Inc.: Hoboken, NJ, 2005.
(26) Lucadamo, G.; Medlin, D. L. Geometric origin of hexagonal close packing at a grain boundary in gold. *Science* **2003**, *300*, 1272−1275.